Fiber-Coupled THz TDS System With mW-Level THz Power and up to 137-dB Dynamic Range

Alexander Dohms ⬤, Nico Vieweg, Steffen Breuer ⬤, Tina Heßelmann, Robert Herda ⬤, Nadja Regner, Shahram Keyvaninia ⬤, Marko Gruner, Lars Liebermeister, Martin Schell, and Robert B. Kohlhaas ⬤

Abstract—Terahertz (THz) time-domain spectroscopy (TDS) offers considerable potential for a wide range of industrial applications, including thickness determination and defect identification through imaging. Fiber-coupled THz TDS systems are particularly promising due to their flexible and robust operation in a variety of environments. However, increasing the THz power of these systems remains a critical challenge for applications that require high dynamic range in very short acquisition times. Here, we present a significant improvement of a commercially available THz TDS system by combining a novel ultrafast Er-doped fiber laser and improved iron-doped InGaAs photoconductive THz emitters. The Er-doped fiber laser offers the combination of high average power up to 70 mW and ultrashort pulse duration down to 45 fs with a fiber delivery of 6.3 m to the THz antennas. The THz emitters are optimized in terms of the photoconductive material and gap size for excitation at optical power >50 mW and provide up to (958 ± 67) μW of emitted THz power. These improvements enable a record peak dynamic range of 117 dB for 60-s acquisition time and the highest peak dynamic range ever measured in a THz TDS setup of 137 dB.

Index Terms—Er-doped fiber laser, high dynamic range (DNR), high power, photoconductive antenna (PCA), terahertz (THz) time-domain spectroscopy (TDS), ultrafast.

I. INTRODUCTION

TERAHERTZ (THz) time-domain spectroscopy (TDS) is a widely used technique in fundamental science and applied research and has also become a promising technique for industrial applications [1], [2]. This is due to its ability to measure multilayer thicknesses, perform noncontact and nondestructive testing and image materials that are transparent in the THz range [3], [4]. However, the applicability of THz TDS in industrial environments depends strongly on the ability to obtain high signal-to-noise ratio within short measurement times. Therefore, the implementation of robust and fast measurement schemes with high THz power is a critical requirement and has emerged as an important area of research.

In recent publications, close to watt-level THz sources have been demonstrated based on optical rectification in nonlinear crystals and two-color plasma filaments [5], [6]. Furthermore, it has been shown that the combination of multi-milliwatt (mW) THz sources with photoconductive receivers based on erbium arsenide (ErAs)-doped InAlGaAs can provide very high dynamic range (DNR) of 115 dB within short measurement times of 120 s [7]. However, the aforementioned THz sources typically suffer from very low conversion efficiencies of 0.1–0.2 % and, thus, require optical excitation pulses with very high energies of tens to hundreds of microjule. So far, this can only be achieved by large custom-built free-space laser systems. Consequently, the deployment of these THz TDS systems in industrial settings is not feasible.

In contrast, fiber-coupled photoconductive THz emitters have demonstrated the potential to achieve much higher optical-to-THz conversion efficiencies of up to 3.4 %, as demonstrated with Rh-doped InGaAs (InGaAs:Rh) for 1550 nm excitation [8]. Current state-of-the-art emitters based on this material system have shown high THz power for photoconductive antennas (PCAs) of (0.97 ± 0.7) mW using 55-mW excitation power at 100-MHz repetition rate, corresponding to only 0.55 nJ excitation energy per pulse [9]. Furthermore, the ability of PCAs to be excited at very high repetition rates from hundreds of megahertz up to the gigahertz regime [10] enables very high DNR. In recent publications, the combination of PCA emitter and receiver made of ErAs-doped In(Al)GaAs superlattice achieved 110 dB in 60-s integration time [11], while 111 dB was obtained within 120 s from optimized PCAs made of InGaAs:Rh [8].

The aforementioned properties of PCAs make it possible to operate them with pulse energies below 1 nJ and, hence, facilitate their integration with mature optical fiber technology at 1550 nm. The resulting all-fiber-coupled THz TDS systems benefit from compact and robust Er-doped fiber lasers and off-the-shelf standard telecom components, which makes them compact, reliable, and cost effective and, thus, ready to use in industrial environments [12], [13], [14].

However, commercially available systems are still limited to THz powers below 100 μW, restricting their accessible DNR to typically 100 dB in 60-s integration time. Here, we investigate on how to enhance the available THz power of such systems in order

to boost the DNR. To achieve this, we have improved two key components: at first, we introduce a novel Er-doped fiber laser optimized for ultrashort pulse duration at high average optical power and its implementation into a commercially available THz TDS system. Then, we investigate photoconductive emitters based on iron-doped InGaAs (InGaAs:Fe), which has shown great potential as THz emitters and allows for more straight-forward epitaxial growth when compared to InGaAs:Rh due to the much lower effusion cell temperatures required to achieve the desired high doping concentrations of $10^{19} - 10^{20}$ cm^{-3} ($T_{Fe} \sim 1300$ °C and $T_{Rh} \sim 1800$ °C). Here, we optimize the photoconductive material and the antenna gap to make use of the enhanced optical power. Finally, we demonstrate the THz performance of the optimized system combining laser source and the photoconductive THz emitter.

II. LASER AND TDS SYSTEM

Fiber-coupled THz TDS systems offer a number of advantages, including the generation of broadband THz radiation, coherent detection, and turnkey operation [12], [13]. Furthermore, they are designed to offer a high degree of freedom for the positioning of the fiber-coupled measurement heads, which is a critical requirement for many industrial applications. This can involve up to 10 m fiber delivery, allowing the spectrometer to be placed at a considerable distance from the sample under test.

A key component in any THz TDS setup is the laser source, which typically is an Er-doped femtosecond fiber laser. These lasers offer pulse durations down to a few tens of femtoseconds, combined with large spectral bandwidth [15], [16]. However, a major challenge is the transmission of femtosecond laser pulses through several meters of fiber delivery, as required for flexible position of the measurement heads. Here, chromatic dispersion in fibers causes a temporal pulse broadening and, therefore, has to be precompensated in order to obtain ultrashort pulses at the photoconductive emitter and receiver (Tx and Rx). Moreover, nonlinear effects, such as self-phase and cross-phase modulation as well as four-wave mixing, become relevant at high peak intensities. These effects alter the pulse temporal and spectral shape and, therefore, have to be managed correctly to prevent unwanted distortion, i.e., to obtain the desired pulse characteristics.

Here, we introduce a novel oscillator-delay-amplifier scheme, which allows us to circumnavigate the aforementioned effects [17]. The scheme is outlined in Fig. 1. It is based on a fiber oscillator, which is pumped by an external diode and uses an additive-pulse mode-locking scheme [18]. The oscillator provides optical pulses at 1560 nm central wavelength with 16.5 nm bandwidth and 250 fs transform-limited pulse duration at 8-mW average power. The repetition rate of 80 MHz is determined by the length of the fiber ring. The extracted pulses are fed through an isolator and then split into two arms for Tx and Rx, respectively. At this point, a commercially available TDS system (TeraFlash pro, TOPTICA Photonics) is used to introduce the time delay between the and Rx. The spectrometer features a mechanical delay stage in the Rx arm to compensate for the
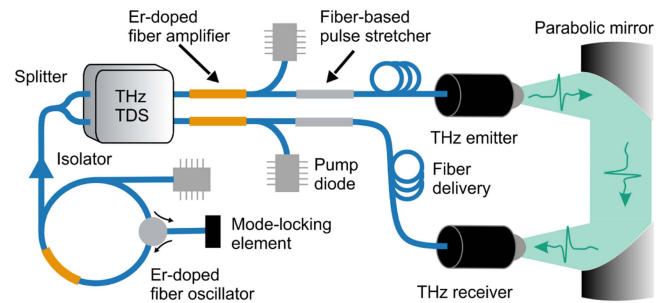

Fig. 1. THz TDS setup: Optical pulses centered at 1550 nm are obtained from a mode-locked Er-doped fiber ring oscillator. The average power is boosted by Er-doped fiber amplifiers, while fiber-based pulse stretchers precompensate the 6.3-m fiber delivery. The time delay between optical excitation of the THz emitter and the receiver module (Tx and Rx) is adjusted with a commercial THz TDS system (TeraFlash pro, TOPTICA Photonics). Emitted THz pulses from the Tx are collimated and focused on the Rx (or pyroelectric detector) by two off-axis parabolic mirrors.

THz free-space path and a mechanical shaker in the Tx arm, with up to 200-ps scan range and 50 fs step size.

After introducing the delay between Rx and Tx, the optical power in both the arms is increased by Er-doped fiber amplifiers. This amplification also significantly broadens the pulse spectrum, mostly due to self-phase modulation in the fiber. At this point, this is a highly desirable effect, since the enhanced bandwidth allows for further compression of the optical pulses to durations below the Fourier limit of the seed spectrum. However, before pulse compression, the pulses have to be precompensated for fiber delivery (here 6.3 m). For this purpose, fiber-based pulse stretchers are used, which introduce normal group velocity dispersion and thereby increase the pulse duration and reduce the peak intensity significantly. In this way, unwanted nonlinear effects are prevented, and the anomalous dispersion of regular polarization-maintaining fibers at 1560 nm can be used to compress the pulses during fiber delivery.

Fig. 2 summarizes the laser characteristics of the TDS system. The average optical power obtained from the Tx and Rx arms increases slightly sublinearly with the pump current and reaches maximum values of 58 and 48 mW, respectively [see Fig. 2(a)]. Note that the laser itself, i.e., without THz spectrometer inserted into the fiber optical path, provides up to 70 mW in the Tx arm and 60 mW in the Rx arm. This difference is due to coupling losses in the free-space delay and shaker unit of the spectrometer, which reduce the available power in the subsequent fiber amplifiers. However, placing the fiber amplifiers after the delay lines of the spectrometer has the critical advantage of feeding high-power optical pulses through less amount of fiber, resulting in fewer pulse distortions.

Fig. 2(b) shows the pulse spectra of Tx and Rx arms at maximum pump current. The spectra are broadband with about 100 nm bandwidth at the −10-dB level. Fig. 2(c) shows the corresponding pulse durations: the Tx arm delivers pulses with 45 fs pulse duration, while the Rx arm provides slightly longer pulses with 54-fs duration, which is probably caused by noncompensated inhomogeneities in the delivery fiber. This combination of high average power of up to 58 mW in conjunction with
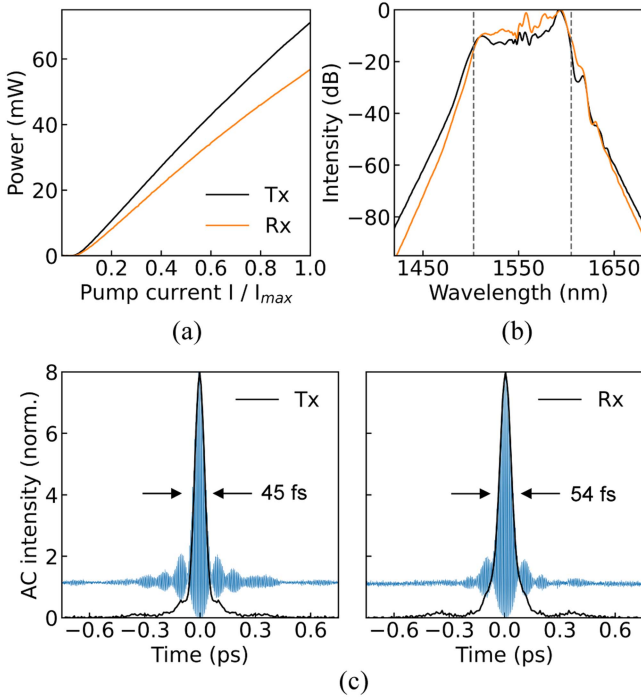
Fig. 2. Laser characteristics after 6.3-m fiber delivery. (a) Average optical power as a function of the normalized pump current ($I/I_{\max}$). (b) Optical spectra of the emitter and receiver path (Tx and Rx). (c) Measured intensity autocorrelation (AC) (black) and interferometric AC (blue) of the Tx and Rx arms at maximum optical power of 70 and 60 mW, respectively.

ultrashort pulse duration as low as 45 fs after 6.3 m of fiber delivery represents excellent values for fiber-coupled THz TDS systems.

III. PHOTOCONDUCTIVE EMITTERS

The key components of fiber-coupled THz TDS systems are the PCAs, which serve as the emitter and the receiver. In photoconductive emitters, THz radiation is generated by the time-varying current that is caused when accelerating photoexcited carriers by an external bias field. Consequently, the emitted electric field E_{THz} can be written as

$$E_{\mathrm{THz}} \propto e\, \frac{dj}{dt} = e\left(n\frac{dv}{dt} + v\frac{dn}{dt}\right) \tag{1}$$

where e is the elementary charge, $j(t)$ is the current density, $n(t)$ is the excited carrier density, and $v(t)$ is the carrier velocity [19]. Here, the contribution of the holes can be omitted, since their effective mass is significantly larger than that for electrons (for $\mathrm{In}_{0.53}\mathrm{Ga}_{0.47}\mathrm{As}$ [20], $m_e = 0.041 m_0$ and $m_h = 0.363 m_0$). From (1), we can conclude four requirements to increase the emitted THz amplitude and, hence, THz power from PCAs: first, the excited electron density $n(t)$ should be maximized by optimizing the PCA material for efficient absorption. Moreover, increasing the optical excitation power will result in larger $n(t)$, which however requires to increase the critical damage threshold of the antennas accordingly. Second, large breakdown field strengths are required to allow high external bias fields E_{bias} for strong acceleration of the photoexcited electrons, i.e., for increasing

dv/dt. At the same time, increasing the external bias field enables higher electron velocities $v = \mu E_{\mathrm{bias}}$, given that the mobility remains constant at high electric field operation, which is the third requirement. Finally, a fast rising and decaying electron density dn/dt will lead to large THz pulse amplitude [21]. This term is governed by two processes: the generation rate of electron–hole pairs is determined by the rising slope of the excitation pulse and, hence, its duration, while the electron–hole recombination is due to the intrinsic carrier lifetime of the photoconductive material.

Over the past few decades, many different material systems have been investigated with respect to the aforementioned requirements, such as low-temperature-grown [22], [23] and ion-implanted [24], [25] semiconductors as well as semiconductor multilayer heterostructures [11], [26], [27]. In general, point defects are introduced to reduce the electron lifetime, which however also act as scattering sites, reducing the carrier mobility. Therefore, the major challenge is the tradeoff between short electron lifetime and high mobility.

Today, state-of-the-art THz TDS systems employ antennas based on InGaAs grown lattice matched on InP to provide efficient absorption at 1550 nm excitation [12]. Furthermore, the electronic and optical properties of InGaAs-based PCAs can be finely adjusted by introducing transition metals, such as rhodium or iron into the crystal lattice. This has been shown to provide unique combinations of very high electron mobility, high sheet resistivity, and ultrashort electron lifetime at the same time [28], [29].

However, efforts to improve the photoconductive material have so far focused on low optical excitation power <30 mW. Moreover, the potential for optimizing the photoconductive gap size for high-power operation has not yet been fully explored. Therefore, this section will first investigate the optimal size of the photoconductive gap for increased excitation power, before demonstrating the pivotal role of the photoconductive material for efficient high-power THz generation.

A. THz Antenna Design

We fabricated THz emitters based on InGaAs:Fe grown by gas-source molecular beam epitaxy [28]. The structure consists of 600 nm nominally undoped InAlAs and 1200 nm InGaAs:Fe grown lattice-matched to a semi-insulating InP:Fe substrate. The InGaAs layer was mesa-structured by photolithography [30] and then equipped with a stripline antenna by metal sputtering. Here, the gap size of the antenna was varied to 25, 35, and 50 μm to investigate the influence of the photoconductive gap on the emitted THz power. For all the measurements, we used fiber-coupled THz emitter modules to allow for compatibility with commercial THz TDS systems.

We measured the THz power from our emitter modules with the setup depicted in Fig. 1. For this purpose, we replace the shown THz receiver module with a pyroelectric thin film detector calibrated by the German metrology institute Physikalisch-Technische Bundesanstalt (PTB). The measurement principle is explained in detail in [31]. Absorbed THz radiation in the detector results in a temperature shift, which in turn causes a
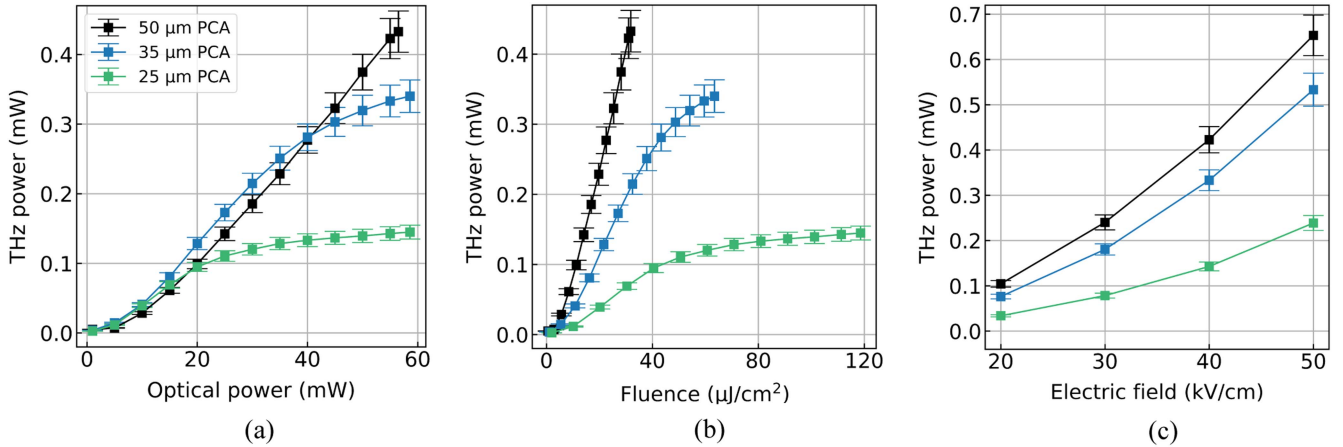
Fig. 3. Comparison of PCAs: measured THz power from PCA emitters with different gap sizes of 25, 35, and 50 µm as a function of (a) the optical excitation power, (b) the incident fluence on the PCA gap, and (c) the applied external electric field. In (a) and (b), the external electric field is 40 kV/cm for all antennas, while in (c), the optical excitation power is 55 mW for all antennas to ensure comparability. The error bars to the measured THz power are derived from the detector uncertainty that amounts to 10 V/W.

change in the electrical potential of the pyroelectric film. This signal from the pyroelectric detector is then amplified by a transimpedance amplifier and measured using an oscilloscope. The responsivity is calibrated by the PTB and was measured as (148 ± 10) V/W at 10^9 A/V amplification. However, the detector is also sensitive for infrared light as well as thermal radiation. Therefore, we modulate the generated THz radiation from the emitter by chopping the electric bias field with a frequency of 25 Hz. This allows us to subtract the static background caused by residual laser power and thermal radiation.

Fig. 3(a) shows the THz power as a function of the optical excitation power P_{opt} measured for the three different gap sizes. To ensure comparability, the same field strength of 40 kV/cm was used for these measurements. For all the gap sizes, the THz power increases linearly up to 20-mW optical power. However, upon increasing P_{opt} further, a significant saturation was observed for the 25 µm-gap antenna, which led to a second linear regime with only little increase in THz power. Therefore, the maximum THz power for this antenna was constrained to 147 µW at 58-mW excitation power. In contrast, the 35- and 50 µm-gap antennas maintained linearity above 20 mW. As shown, the 35 µm-gap antenna performs slightly better than the 50 µm-gap antenna but then saturates from 35 mW onwards, resulting in a maximum THz power of 350 µW. The 50 µm-gap antenna keeps a linear increase in THz power throughout and achieves a maximum value of 433 µW at 56.5 mW optical power (and 40 kV/cm). Consequently, the 50 µm-gap antenna is the optimal choice for operation with enhanced power.

To further investigate the saturation of the antennas with smaller gap size, we converted the optical power to the fluence incident on the PCA. For this purpose, we used a commercial optical backscatter reflectometer (OBR 4600, Luna Innovations) to measure the distance of fiber tip to antenna surface. When assuming the propagation of a Gaussian beam, these distances correspond to spot diameters of 40, 51 and 64 µm on the PCAs with 25-, 35- and 50 µm-gap sizes, respectively. Thus, the excitation spots exceed the corresponding gap sizes slightly. From

our observations, this is the most efficient configuration for THz generation, since the high-intensity part of the lateral Gaussian beam profile is within the PCA gap, while the low-intensity wings with smaller contribution to the emitted THz pulse lie outside of the photoconductive gap.

Fig. 3(b) shows the measured THz power for all the gap sizes as a function of the incident fluence. It is evident that the 25 and 35 µm-gap antennas saturate at the same fluence of 40 µJ/cm². This implies that their performance at higher fluence is restricted by the same saturation effect. In a previous work by Jepsen et al. [19], it was shown that this saturation can be attributed to screening of the external bias field by space charge separation in the photoconductor. This effect becomes more pronounced for higher excited carrier densities [19], which was likewise observed for large-area photoconductive emitters [32]. Therefore, the THz power emitted from the 25- and 35 µm-gap antennas presented in this work is limited by the small excitation spot on the photoconductor, which leads to comparably higher excited carrier densities. In this regard, the 50 µm-gap antenna benefits from the larger spot size, which here prevents exceeding the critical fluence of 40 µJ/cm². Based on these measurements, we conclude that the 50 µm-gap antenna may be driven with up to 70-mW excitation power before showing saturation.

In the last step, we have measured the dependence of the emitted THz power on the applied external bias field E_{bias} at constant excitation power of 55 mW [see Fig 3(c)]. Clearly, all the antennas exhibit a quadratic increasing THz power in the measured range. This is to be expected from (1), which can be rewritten in terms of the bias field, since $j = \sigma E_{\mathrm{bias}}$ with σ being the time-dependent conductivity $\sigma = env$. Therefore, we find $E_{\mathrm{THz}} \propto \dot{\sigma} E_{\mathrm{bias}}$ and, thus, a quadratic dependence of the THz power with the applied electric field, i.e., $P_{\mathrm{THz}} \propto E_{\mathrm{bias}}^2$ [33]. Here, the 50 µm-gap performs best, reaching a maximum emitted THz power of 653 µW. The smaller gap antennas with 25- and 35 µm-gap are operated in saturation at this excitation power and, hence, provide lower maximum THz power of 238 and 533 µW, respectively.
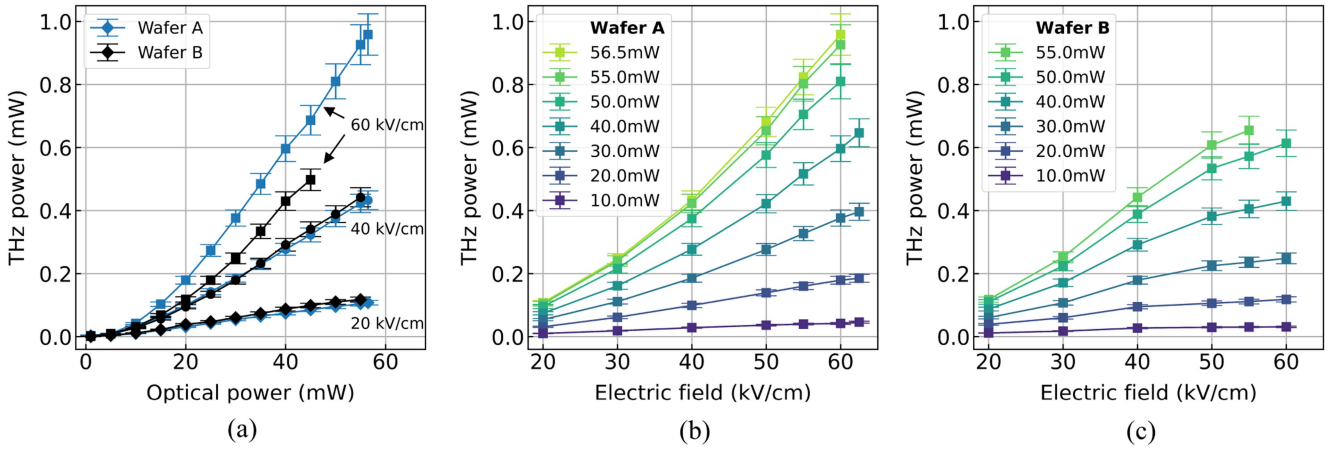
Fig. 4. Comparison of photoconductive material: measured THz power from PCA emitters with 50 μm-gap size from two different wafers (A and B) as a function of (a) the optical power for different electric field strengths and (b) and (c) of the electric field for different optical powers for the two wafers. The THz power measured from wafer B saturates above 40 kV/cm, resulting in a maximum value of 654 μW. Wafer A maintains a linear increase in THz power and achieves a maximum value of (958 ± 67) μW.

B. Photoconductive Material

In this section, we investigate the effect of the material properties of InGaAs:Fe on the emitted THz power. For this purpose, we compare the performance of THz emitters with 50 μm-gap antenna from two wafers with different electronic and optical properties. The two wafers were grown with a nominal iron doping concentration of 1.2×10^{20} cm^{-3} but different growth temperatures of 390 °C for wafer A and 440 °C for wafer B. We measured their Hall mobility μ, free electron concentration n_0, and sheet resistance R using a commercial Hall measurement setup (Accent HL5500PC). Moreover, the characteristic electron lifetime $\tau_{1/e}$ was determined in a time-differential pump-probe setup at 1550 nm. Here, the electron lifetime is defined as the time Δt after photoexcitation with a femtosecond pump pulse at which the transmission for the probe pulse drops to $1/e$ of the maximum transmission $(T_{\max} = T(\Delta t = 0))$. This corresponds to the time at which $1/e$ of the overall photoexcited electrons n have been trapped in a midgap defect state (Fe-state) or recombined, i.e., they no longer contribute to the conductivity.

The measured material properties are given in Table I. Both wafers, A and B, show very high mobility of 1517 and 900 cm^2/V·s, combined with ultrashort carrier lifetime of 0.54 and 0.96 ps, respectively. However, wafer A shows a one order of magnitude lower free electron concentration n_0 of 2.3×10^{12} cm^{-3} and, hence, a higher sheet resistance of 1820 Ω·cm compared with wafer B.

Fig. 4(a) shows the measured THz power from the two wafers as a function of the optical excitation power for different electric field strengths. It can be seen that the two wafers perform equally well up to 40 kV/cm, both showing linear slopes with almost identical THz power levels. However, when comparing the measured THz power for the two wafers as a function of the electric field strength [see Fig. 4(b) and (c)], we observe a pronounced saturation for wafer B above 40 kV/cm. In particular, we find that the measured THz power does no longer increase quadratically with the bias field independently of the optical excitation power.

TABLE I
MATERIAL PROPERTIES OF INGAAS:FE SAMPLES

Wafer	μ (cm^2/V·s)	n_0 (cm^{-3})	R (Ω·cm)	$\tau_{1/e}$ (ps)
A	1517	2.3×10^{12}	1820	0.54
B	900	1.3×10^{13}	532	0.96

As a result, the measured THz powers of the two wafers diverge beyond 40-kV/cm field strength and already differ by 148 μW at 55 kV/cm and 55-mW excitation power. Here, wafer B has its maximum of 654 μW, as a further increase in optical power destroyed the antenna. In contrast, wafer A maintains a quadratic increase in THz power with the electric field strength and reaches a maximum emitted THz power of 958 μW at 60 kV/cm and 56.5-mW excitation power. This is an outstanding value that reaches the mW range and has been so far only achieved with similar antennas based on InGaAs:Rh [9].

We attribute the higher damage threshold of wafer A compared with wafer B to two main features: first, the very high resistivity of wafer A limits the average current density, both in DC mode and under illumination. Second, photoexcited electrons are trapped much faster in wafer A due to its much shorter electron lifetime when compared with wafer B. This further reduces the current density during and shortly after illumination. As a result, wafer A experiences a much lower thermal load due to less carrier scattering with other carriers, crystal impurities, and phonons and is, therefore, less susceptible to current runaway due to excessive intrinsic carrier generation. This should significantly enhance the critical damage threshold of this wafer compared with wafer B.

The saturating THz power from wafer B above 40 kV/cm may likewise be caused by the higher thermal load, i.e., higher intrinsic temperature in this wafer at high bias fields. In particular, an increasing carrier–phonon scattering rate may result in a saturation of the electron velocity, i.e., a deviation from the linear relation $v = \mu E$, due to a decreasing mobility. In addition to this,
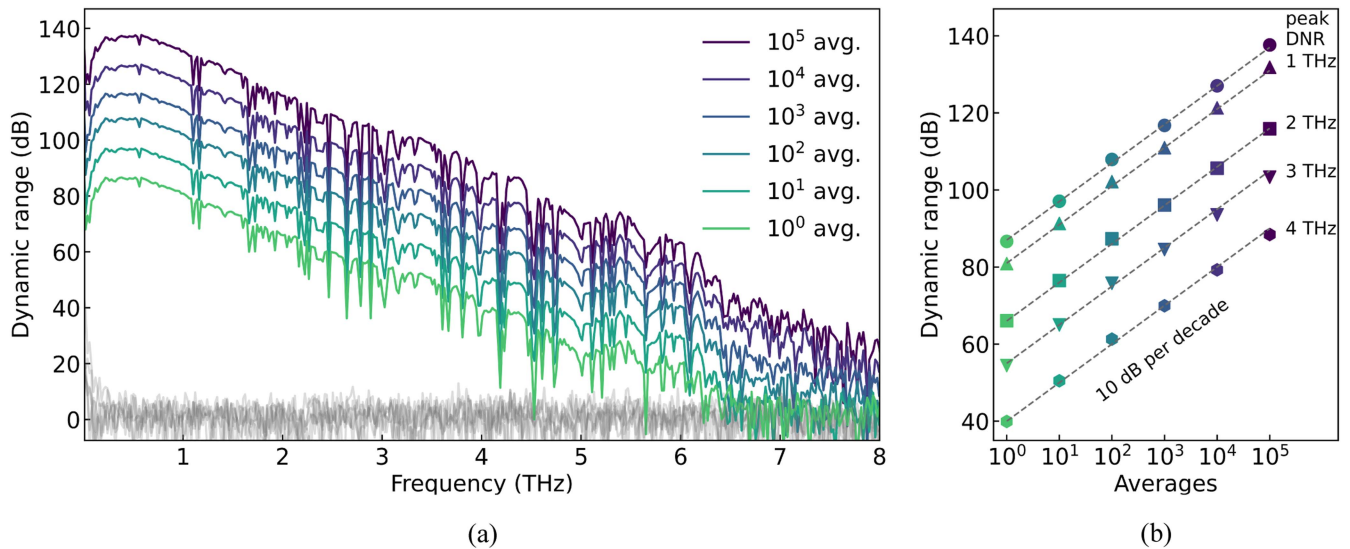
Fig. 5.   (a) THz power spectra obtained for different number of averages. The measurements were taken with an InGaAs:Fe stripline emitter with a 50 μm gap biased at 40 kV/cm and an InGaAs:Rh-based receiver with a 20 μm gap. The emitter and receiver were illuminated with 55- and 45-mW optical excitation power. The noise level was obtained by blocking the THz path. (b) DNR as a function of averages: The DNR increases by 10 dB for every decade of averages (dashed lines) for all frequencies, proving stable system operation without drift up to 10^5 averages (100-min measurement time). A record value of 137-dB peak DNR was achieved.

wafer A already shows much higher DC mobility, which is a good indicator of how well the transport takes place under illumination. Another possible reason for the saturation of the THz power from wafer B could be the rising rate of carrier generation at higher intrinsic temperature. The higher carrier density may decrease the critical fluence, at which carrier screening results in a reduced effective bias field. However, this would imply that the saturation of the emitted THz power depends on the optical power, which we do not observe.

IV. TDS System Performance

In this section, we demonstrate the THz performance of a commercial TDS system (TeraFlash pro, TOPTICA Photonics) modified with the two key components optimized in this work: the high-power ultrafast Er-doped fiber laser and the InGaAs:Fe THz emitters designed for high-power operation. For this purpose, we measure THz spectra using the 50 μm-gap emitter from wafer A, presented in the previous section, in combination with state-of-the-art InGaAs:Rh receivers [34] in the setup configuration depicted in Fig. 1. Here, the optical excitation powers for the Tx and the Rx were set to 55 and 45 mW, respectively, while the Tx was biased with 40 kV/cm. At this field strength, about 400-μW THz power is available, and we do expect no device degradation during long-term operation. Therefore, the following measurement results are a good indicator for the system performance in real-world applications.

Fig. 5(a) shows the measured THz power spectra for different averaging modes, from single shot, i.e., a single sampling of the pulse trace, up to 10^5 averages. The DNR was determined by normalizing the power spectrum to the receiver noise spectrum. The receiver noise was obtained by blocking the THz path and measuring the receiver signal with the same number of averages.

In single-shot mode, the TDS system samples the entire pulse trace in just 60 ms, which already provides 87 dB in peak DNR and 6.5-THz bandwidth. Upon increasing the number of averages by a factor of 10, we measure a 10-dB increase in the DNR across the spectrum, as expected from theory. This is depicted in Fig. 5(b), which shows the DNR at different frequencies as well as the peak DNR plotted against the number of averages on a logarithmic scale. Clearly, the DNR for all the frequencies increases linearly up to 10^5 averages (100-min measurement time), as indicated by the dashed lines, which represent a 10-dB increase per decade of averages. From this, we conclude that our THz TDS system operates stable with negligible drift throughout the entire measurement time. At this point, it is worth noting that for 10^3 averages or more, a signal at higher frequencies >6.5 THz can be observed, which does not show the expected water absorption lines in this frequency range, while the spectrum up to 6.5 THz is unaffected from this effect.

A record peak DNR of 117 dB is achieved for 60-s integration time (1000 averages). This is a 7-dB increase to state-of-the-art fiber-coupled TDS systems employing PCAs made of ErAs-doped In(Al)GaAs superlattices with the same integration time [11] and a 6-dB improvement over PCAs made from InGaAs:Rh within twice the integration time of 120 s [8]. Moreover, to the best of our knowledge, we achieve the highest peak DNR ever measured with a TDS system: at 100-min integration time (10^5 averages), our modified TDS system provides 137 dB in peak DNR without any further postprocessing. This outperforms the current state-of-the-art by 4 dB, which was, however, measured with a much longer integration time of 390 min and postprocessed with an interferometric reference signal to reconstruct the delay axis [35].

V. CONCLUSION

In conclusion, we have presented a fiber-coupled THz TDS system with mW-level THz power and up to 137-dB DNR. This is the highest DNR for THz TDS reported in the literature, so far. To achieve this, we used a novel Er-doped fiber laser based on an oscillator-delay-amplifier scheme, which can be easily integrated into commercially available THz TDS systems. In our THz TDS setup, this laser achieves a unique combination of high average optical power up to 58 mW and ultrashort pulse duration down to 45 fs after a fiber delivery of 6.3 m. In addition, we have developed THz emitters based on InGaAs:Fe that are suitable for excitation with optical power above 50 mW. These emitters feature a 50 µm photoconductive gap to prevent the saturation of the emitted THz power at high optical power due to screening of the electric bias field. Moreover, we have shown that high resistivity and ultrafast carrier trapping play a pivotal role for fabricating a robust and efficient photoconductive THz emitter. Clearly, the combination of our ultrafast Er-doped fiber laser and InGaAs:Fe photoconductive THz emitter is a significant improvement for high-speed and high-DNR fiber-coupled THz TDS systems for fast-paced industrial applications.

REFERENCES

[1] P. Jepsen, D. G. Cooke, and M. Koch, "Terahertz spectroscopy and imaging—Modern techniques and applications," *Laser Photon. Rev.*, vol. 5, pp. 124–166, Jan. 2011.

[2] M. Naftaly, N. Vieweg, and A. Deninger, "Industrial applications of terahertz sensing: State of play," *Sensors*, vol. 19, Sep. 2019, Art. no. 4203.

[3] D. Molter et al., "Kilohertz pixel-rate multilayer terahertz imaging of subwavelength coatings," *Appl. Sci.*, vol. 12, May 2022, Art. no. 4964.

[4] S. Krimi et al., "Highly accurate thickness measurement of multi-layered automotive paints using terahertz technology," *Appl. Phys. Lett.*, vol. 109, Jul. 2016, Art. no. 021105.

[5] J. Buldt et al., "Gas-plasma-based generation of broadband terahertz radiation with 640 mW average power," *Opt. Lett.*, vol. 46, pp. 5256–5259, Oct. 2021.

[6] T. Vogel, S. Mansourzadeh, and C. J. Saraceno, "Single-cycle, 643 mW average power terahertz source based on tilted pulse front in lithium niobate," *Opt. Lett.*, vol. 49, pp. 4517–4520, Aug. 2024.

[7] T. Vogel et al., "Performance of photoconductive receivers at 1030 nm excited by high average power THz pulses," *IEEE Trans. THz Sci. Technol.*, vol. 14, no. 2, pp. 139–151, Mar. 2024.

[8] R. B. Kohlhaas et al., "637 µW emitted terahertz power from photoconductive antennas based on rhodium doped InGaAs," *Appl. Phys. Lett.*, vol. 117, 2020, Art. no. 131105.

[9] R. B. Kohlhaas et al., "Fiber-coupled THz TDS system with mW-level THz power," in *Proc. IEEE 47th Int. Conf. Infrared, Millimeter THz Waves*, 2022, pp. 1–2.

[10] B. Willenberg et al., "Rapid THz-TDS enabled by single-cavity dual-comb gigahertz laser," *EPJ Web Conf.*, vol. 267, 2022, Art. no. 01038.

[11] U. Nandi et al., "Bias-dependent carrier dynamics and terahertz performance of ErAs:In(Al)GaAs photoconductors," *IEEE Trans. THz Sci. Technol.*, vol. 12, no. 4, pp. 353–362, Jul. 2022.

[12] N. Vieweg et al., "Terahertz-time domain spectrometer with 90 dB peak dynamic range," *J. Infrared, Millimeter, THz Waves*, vol. 35, pp. 823–832, Jul. 2014.

[13] R. J. B. Dietz et al., "All fiber-coupled THz-TDS system with kHz measurement rate based on electronically controlled optical sampling," *Opt. Lett.*, vol. 39, pp. 6482–6485, Nov. 2014.

[14] M. Yahyapour et al., "Fastest thickness measurements with a terahertz time-domain system based on electronically controlled optical sampling," *Appl. Sci.*, vol. 9, Mar. 2019, Art. no. 1283.

[15] D. Brida, G. Krauss, A. Sell, and A. Leitenstorfer, "Ultrabroadband Er: fiber lasers," *Laser Photon. Rev.*, vol. 8, pp. 409–428, Jan. 2014.

[16] W. Hänsel et al., "All polarization-maintaining fiber laser architecture for robust femtosecond pulse generation," *Appl. Phys. B*, vol. 123, Jan. 2017, Art. no. 41.

[17] Toptica Photonics AG, "Fiber delivery of short laser pulses," U.S. Patent US9 882 342 B2, 2018.

[18] J. Kim and Y. Song, "Ultralow-noise mode-locked fiber lasers and frequency combs: Principles, status, and applications," *Adv. Opt. Photon.*, vol. 8, pp. 465–540, Aug. 2016.

[19] P. U. Jepsen, R. H. Jacobsen, and S. R. Keiding, "Generation and detection of terahertz pulses from biased semiconductor antennas," *J. Opt. Soc. Amer. B*, vol. 13, pp. 2424–2436, Nov. 1996.

[20] S. Adachi, *Physical Properties of III-V Semiconductor Compounds: InP, InAs, GaAs, GaP, InGaAs, and InGaAsP*. Hoboken, NJ, USA: Wiley, 1992.

[21] Z. Piao, M. Tani, and K. Sakai, "Carrier dynamics and terahertz radiation in photoconductive antennas," *Jpn. J. Appl. Phys.*, vol. 39, Jan. 2000, Art. no. 96.

[22] J. Sigmund et al., "Structure investigation of low-temperature-grown GaAsSb, a material for photoconductive terahertz antennas," *Appl. Phys. Lett.*, vol. 87, Dec. 2005, Art. no. 252103.

[23] J. M. Rämer, F. Ospald, G. von Freymann, and R. Beigang, "Generation and detection of terahertz radiation up to 4.5 THz by low-temperature grown GaAs photoconductive antennas excited at 1560 nm," *Appl. Phys. Lett.*, vol. 103, Jul. 2013, Art. no. 021119.

[24] M. Suzuki and M. Tonouchi, "Fe-implanted InGaAs terahertz emitters for 1.56µm wavelength excitation," *Appl. Phys. Lett.*, vol. 86, Jan. 2005, Art. no. 051104.

[25] N. Chimot et al., "Terahertz radiation from heavy-ion-irradiated In0.53Ga0.47As photoconductive antenna excited at 1.55µm," *Appl. Phys. Lett.*, vol. 87, Nov. 2005, Art. no. 193510.

[26] P. W. Juodawlkis, D. T. McInturff, and S. E. Ralph, "Ultrafast carrier dynamics and optical nonlinearities of low-temperature-grown InGaAs/InAlAs multiple quantum wells," *Appl. Phys. Lett.*, vol. 69, pp. 4062–4064, 1996.

[27] R. J. B. Dietz et al., "THz generation at 1.55 µm excitation: Six-fold increase in THz conversion efficiency by separated photoconductive and trapping regions," *Opt. Exp.*, vol. 19, pp. 25911–25917, Dec. 2011.

[28] B. Globisch et al., "Iron doped InGaAs: Competitive THz emitters and detectors fabricated from the same photoconductor," *J. Appl. Phys.*, vol. 121, 2017, Art. no. 053102.

[29] R. B. Kohlhaas et al., "Rhodium doped InGaAs: A superior ultrafast photoconductor," *Appl. Phys. Lett.*, vol. 112, Mar. 2018, Art. no. 102101.

[30] H. Roehle et al., "Next generation 1.5 µm terahertz antennas: Mesa-structuring of InGaAs/InAlAs photoconductive layers," *Opt. Exp.*, vol. 18, pp. 2296–2301, Jan. 2010.

[31] B. Globisch et al., "Absolute terahertz power measurement of a time-domain spectroscopy system," *Opt. Lett.*, vol. 40, pp. 3544–3547, Jul. 2015.

[32] M. Beck et al., "Impulsive terahertz radiation with high electric fields from an amplifier-driven large-area photoconductive antenna," *Opt. Exp.*, vol. 18, pp. 9251–9257, Apr. 2010.

[33] E. Castro-Camus, J. Lloyd-Hughes, and M. B. Johnston, "Three-dimensional carrier-dynamics simulation of terahertz emission from photoconductive switches," *Phys. Rev. B*, vol. 71, May 2005, Art. no. 195301.

[34] R. B. Kohlhaas et al., "Photoconductive terahertz detectors with 105 dB peak dynamic range made of rhodium doped InGaAs," *Appl. Phys. Lett.*, vol. 114, Jun. 2019, Art. no. 221103.

[35] V. Cherniak, T. Kubiczek, K. Kolpatzeck, and J. C. Balzer, "Laser diode based THz-TDS system with 133 dB peak signal-to-noise ratio at 100 GHz," *Sci. Rep.*, vol. 13, Aug. 2023, Art. no. 13476.

Alexander Dohms received the B.Sc. and M.Sc. degrees in physics from the Humboldt University of Berlin, Berlin, Germany, in 2017, and 2021, respectively. He is currently working toward the Ph.D. degree in physics with Fraunhofer Heinrich Hertz Institute (HHI), Berlin.

In 2017, he joined the Fraunhofer HHI as a Research Assistant, where he worked with the Epitaxy Group from 2017 to 2019 and with the Terahertz Sensors and Systems Group from 2019 to 2021. In 2018, he was a Visiting Student Researcher with Osaka City University, Osaka, Japan. Since 2021, he has been a Research Associate with the Terahertz Sensors and Systems Group, Fraunhofer HHI. His research interests include ultrafast photoconductors grown by molecular beam epitaxy, optoelectronic terahertz sources, and receivers as well as semiconductor saturable absorber mirrors for ultrafast lasers.

Nico Vieweg was born in Ueckermuende, Germany, in 1976. He received the B.Sc. and M.Sc. degrees in communication and high-frequency engineering from the Department of Electrical Engineering and Computer Science, Stralsund University of Applied Science, Stralsund, Germany, in 2004 and 2006, respectively, and the Ph.D. degree in electrical engineering in the field of terahertz science and technology from the Institute of High Frequency Technology, Technical University of Braunschweig, Braunschweig, Germany, in 2011.

In 2012, he joined TOPTICA Photonics AG, Gräfelfing, Germany, where he is currently the Director of the R&D Terahertz Systems Group. He has more than ten years of experience in the field of optoelectronic generation and detection of terahertz waves. He authored more than 100 peer-reviewed papers and conference publications as well as a book chapter and holds three patents on terahertz instrumentations. His current research interests include optoelectronic terahertz systems and their use for spectroscopy, sensing, and terahertz communication.

Dr. Vieweg is a Member of the Technical Committee for Terahertz Systems VDI/VDE-GMA FA 8.17 of the Association of German Engineers.

Steffen Breuer received the B.Sc. degree in physics from Durham University, Durham, U.K., in 2002, the Diploma degree in physics from Free University Berlin, Berlin, Germany, in 2006, and the Ph.D. degree (summa cum laude) in physics from Humboldt University Berlin, Berlin, and Paul Drude Institute, Berlin, in 2011.

From 2011 to 2013, he was a Postdoctoral Fellow with Australian National University, Canberra, ACT, Australia, working on III-V nanowires for solar cells. From 2013 to 2016, he was a Postdoctoral Researcher of III-nitride transistor epitaxy with Fraunhofer IAF, Freiburg/Breisgau, Germany. Since 2016, he has been an Epitaxy Scientist with Fraunhofer Heinrich Hertz Institute, Berlin, leading the Molecular Beam Epitaxy (MBE) Lab. His research interests include high-precision semiconductor epitaxy by MBE and metal-organic chemical vapor deposition, development of ultrafast photoconductors for terahertz sources and detectors, and saturable absorber mirrors for ultrafast lasers.

Dr. Breuer received the Lise Meitner Prize for outstanding Ph.D. thesis from Humboldt University Berlin in 2011. He is a Member of the German Physical Society.

Tina Heßelmann was born in Bocholt, Germany. She received the M.Eng. degree in medical physics from Berliner Hochschule für Technik, Berlin, Germany, in 2022. She is currently working toward the Ph.D. degree with the Terahertz Sensors and Systems Group, Fraunhofer Institute for Telecommunications, Heinrich Hertz Institute, Berlin.

Her current research interests include integrated terahertz photonics and optoelectronic terahertz systems and antennas.

Robert Herda received the diploma degree in physics from the Friedrich Schiller University Jena, Jena, Germany, in 2003, and the Doctor of Science degree in physics from the Tampere University of Technology, Tampere, Finland, in 2006.

He then joined TOPTICA Photonics AG, Gräfelfing, Germany. He is a Fellow in R&D Ultrafast Fiber Lasers. His research interests include frequency combs, ultrashort pulse generation in fiber oscillators and amplifiers, and nonlinear optics.

Nadja Regner, photograph and biography not available at the time of publication.

Shahram Keyvaninia received the B.Sc. degree in applied physics and the M.Sc. degree in photonics from the Sharif University of Technology, Tehran, Iran, and the Ph.D. degree in photonics from the Technical University of Berlin, Berlin, Germany.

In 2008, he joined the Photonic Research Group, Interuniversity Microelectronics Center/Ghent University, Ghent, Belgium, and was a Visiting Scientist with the Photonic Integration Group, Technical University of Eindhoven, Eindhoven, The Netherlands. During this time, he developed technology for integrating III–V materials on silicon-on-insulator substrates using die-to-wafer bonding and innovative fabrication processes for photonic devices. Since 2015, he has been a Senior Scientific Researcher with the Fraunhofer Heinrich Hertz Institute, Berlin. His current research interests include the design and fabrication of integrated photonic devices for terahertz and sensing applications.

Dr. Keyvaninia is a Member of the IEEE Laser and Electro-Optics Society and the Optical Society of America.

Marko Gruner, photograph and biography not available at the time of publication.

Lars Liebermeister received the Ph.D. degree in quantum and nanophotonics from Ludwig-Maximilians-Universität Munich, Munich, Germany, in 2016.

Since 2017, he has been the Project Leader and the Deputy Group Leader with the Terahertz Sensors and Systems Group, Fraunhofer Institute for Telecommunications, Heinrich Hertz Institute, Berlin, Germany. His current research interests include integrated terahertz photonics, optoelectronic terahertz systems, and terahertz quantum optics.

Martin Schell received the diploma degree in physics from RWTH Aachen University, Aachen, Germany, in 1989, and the Dr.rer.nat. degree in physics from the Technical University of Berlin, Berlin, Germany, in 1993.

In 1995, he was a Visiting Researcher with the University of Tokyo, Tokyo, Japan. From 1996 to 2000, he was a Management Consultant with the Boston Consulting Group, Boston, MA, USA. From 2000 to 2005, he was a Product Line Manager and then the Head of Production and Procurement with Infineon Fiber Optics, Berlin. He is currently the Director of the Fraunhofer Heinrich Hertz Institute, Berlin, and a Professor of Optic and Optoelectronic Integration with the Technical University of Berlin.

Dr. Schell was a Board Member of the European Photonics Industry Consortium from 2015 to 2021. He is a Chairman of the Competence Network Optical Technologies Berlin/Brandenburg, a Spokesman of the Berlin-Brandenburg Photonics Cluster, and a Member of the Photonics21 Board of Stakeholders.

Robert B. Kohlhaas received the M.Sc. degree in physics and the Ph.D. degree in physics from Technische Universität Berlin, Berlin, Germany, in 2016 and 2021, respectively.

He joined the Fraunhofer Institute for Telecommunications, Heinrich Hertz Institute (HHI), Berlin, as a Research Associate and Project Manager. His Ph.D. research focused on photoconductive antennas for pulsed terahertz (THz) generation and detection. Since 2022, he has been the Head of the Terahertz Sensors and Systems Group, Fraunhofer HHI. He is the author of more than 50 publications in peer-reviewed journals and conference proceedings. His research interests include optoelectronic THz sources and receivers, THz communication links, photonic integrated THz systems, semiconductor saturable absorber mirror (SESAM)s, as well as ultrafast photoconductive materials grown by molecular beam epitaxy.